

Universal controlled-phase gate with cat-state qubits in circuit QED

Yu Zhang¹, Xiong Zhao¹, Li Yu^{1,2}, Qi-Ping Su¹ and Chui-Ping Yang^{1*}

¹*Department of Physics, Hangzhou Normal University,
Hangzhou, Zhejiang 310036, China and*

²*CAS Key Laboratory of Quantum Information,
University of Science and Technology of China, Hefei 230026, China*

(Dated: August 16, 2017)

Abstract

Cat-state qubits (qubits encoded with cat states) have recently drawn intensive attention due to their enhanced life times with quantum error correction. We here propose a method to implement a universal controlled-phase gate of two cat-state qubits, via two microwave resonators coupled to a superconducting transmon qutrit. During the gate operation, the qutrit remains in the ground state; thus decoherence from the qutrit is greatly suppressed. This proposal requires only two basic operations and neither classical pulse nor measurement is needed; therefore the gate realization is simple. Numerical simulations show that high-fidelity implementation of this gate is feasible with current circuit QED technology. The proposal is quite general and can be applied to implement the proposed gate with two microwave resonators or two optical cavities coupled to a single three-level natural or artificial atom.

PACS numbers: 03.67.Bg, 42.50.Dv, 85.25.Cp, 76.30.Mi

*Electronic address: yangcp@hznu.edu.cn

I. INTRODUCTION

Circuit quantum electrodynamics (QED), composed of superconducting (SC) qubits and microwave resonators or cavities, has developed fast in the past decade. The circuit QED is considered as one of the most feasible candidates for quantum information processing (QIP) [1-4]. Due to controllability of their level spacings, scalability of the circuits, and improvement of coherence times [5-12], SC qubits are of great importance in QIP. The strong coupling and ultrastrong coupling between a SC qubit and a microwave resonator have been demonstrated in experiments [13,14]. In addition, a coplanar waveguide microwave resonator with a (loaded) quality factor $Q = 10^6$ [15,16] and a three-dimensional microwave resonator with a (loaded) quality factor $Q \sim 3.5 \times 10^7$ [17] have been reported in experiments. A microwave resonator or cavity with a high quality factor can act as a quantum data bus [18-20] and be used as a quantum memory [21,22], because it contains microwave photons whose life times are much longer than that of a SC qubit [23]. Recently, quantum state engineering and QIP with microwave fields or photons have attracted considerable interest.

Many theoretical proposals have been presented for preparation of Fock states, squeezed states, coherent states, schrödinger cat states, and an arbitrary superposition of Fock states of a single microwave resonator [24-27]. Also, a Fock state and a superposition of Fock states of a single microwave resonator has been created experimentally [21,28,29]. For two microwave resonators, theoretical proposals have been proposed for generation of nonclassical microwave field in two resonators [30-33], construction of two-qubit controlled-phase gates with microwave photons in two resonators [34], and implementation of quantum state transfer between microwave photons in two resonators [35-37]. Experimentally, the creation of N-photon NOON states in two microwave resonators has been reported [38]. A complete quantum state transfer of a microwave photon qubit between two resonators can be experimentally realized, by combination of two previous experiments [39,40] which employed the transfer protocol proposed in Ref. [36]. Moreover, schemes have been proposed for generation of multipartite entangled states of microwave photons in multiple resonators [41] and creation of entangled coherent states of microwave fields in many resonators or cavities [42].

The focus of this work is on QIP with cat-state qubits (qubits encoded with cat states). Cat-state qubits have drawn much attention due to their enhanced life time with quantum error correction (QEC). For instance, Ofek *et al.* have made the lifetime of a cat-state qubit

up to 320 μs with QEC [43]. Recently, there is an increasing interest in QIP with cat-state encoding qubits. Mirrahimi *et al.* have presented approaches to realize a set of universal gates on a single cat-state qubit as well as an entangling gate for creating a Bell state of two cat-state qubits [44]. Nigg has proposed a method for a deterministic Hadamard gate on a single cat-state qubit [45]. Heeres *et al.* have experimentally implemented a set of universal gate on a single cat-state qubit [46]. Yang *et al.* have proposed a scheme for implementing a SWAP gate of two cat-state qubits [47]. Moreover, Wang *et al.* have experimentally generated an entangled Bell state with two cat-state qubits [48]. However, after a deep search of literature, we found that how to realize a controlled-phase gate of two *cat-state* qubits has not been investigated so far. As is well known, a two-qubit controlled phase gate is *universal*, because two-qubit controlled phase gates, together with single-qubit gates, form the building blocks of quantum information processors.

In this paper, we propose a method to realize a universal two-qubit controlled-phase gate with cat-state qubits, via two microwave resonators coupled to a SC transmon qutrit (a three-level artificial atom) (Fig. 1). During the gate operation, the qutrit stays in the ground state; thus decoherence from the qutrit is greatly suppressed. The gate implementation is simple because only two basic operations are needed and no classical pulse or measurement is required. Our numerical simulations show that high-fidelity implementation of this gate is feasible with current circuit QED technology.

This paper is organized as follows. In Sec. II, we explicitly show how to realize a universal controlled-phase gate of two cat-state qubits. In Sec. III, we numerically calculate the fidelity and briefly discuss the experimental feasibility. We end up with a conclusion in Sec. IV.

II. CONTROLLED-PHASE GATE OF CAT-STATE QUBITS

Consider a system consisting of two microwave resonators coupled to a transmon qutrit (Fig. 1). The three level of the qutrit are labeled as $|g\rangle$, $|e\rangle$ and $|f\rangle$, as shown in Fig. 2. It is worth noting that for an ideal transmon, the $|g\rangle \leftrightarrow |f\rangle$ coupling is theoretically zero due to the selection rule [49]; however in practice, there exists a weak coupling between these two states [50]. Supposed that resonator *a* is off-resonantly coupled to the $|g\rangle \leftrightarrow |e\rangle$ transition of the qutrit with coupling constant g while resonator *b* is off-resonantly coupled to the $|e\rangle \leftrightarrow |f\rangle$ transition of the qutrit with coupling constant μ (Fig. 2). In addition,

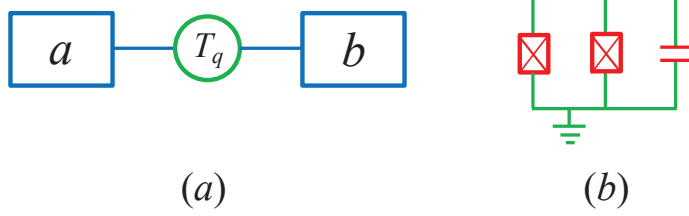


FIG. 1: (Color online) (a) Diagram of two microwave resonators a and b coupled to a transmon qutrit (T_q). Each resonator can be one-dimensional or three-dimensional resonator. The qutrit is capacitively or inductively coupled to each resonator. (b) Electronic circuit of a transmon qutrit, which consists of two Josephson junctions and a capacitor.

assume that resonator a is highly detuned (decoupled) from the $|e\rangle \leftrightarrow |f\rangle$ transition of the qutrit and resonator (b) is highly detuned (decoupled) from the $|g\rangle \leftrightarrow |e\rangle$ transition of the qutrit (Fig. 3). Note that these conditions can be achieved by prior adjustment of the level spacings of the qutrit or/and the resonator frequency. Under these considerations, the Hamiltonian of the whole system, in the interaction picture and after making the rotating-wave approximation (RWA), can be written as (in units of $\hbar = 1$)

$$H_{I,1} = g(e^{i\delta_a t} \hat{a} \sigma_{eg}^+ + h.c.) + \mu(e^{i\delta_b t} \hat{b} \sigma_{fe}^+ + h.c.), \quad (1)$$

where $\sigma_{eg}^+ = |e\rangle\langle g|$, $\sigma_{fe}^+ = |f\rangle\langle e|$, $\delta_a = \omega_{eg} - \omega_a < 0$ and $\delta_b = \omega_{fe} - \omega_b > 0$. The detunings $|\delta_a|$ and $|\delta_b|$ in Fig. 2 are given by $|\delta_a| = \omega_a - \omega_{eg}$ and $|\delta_b| = \omega_{fe} - \omega_b$. Here, \hat{a}^+ (\hat{b}^+) is the photon creation operator of resonator a (b), ω_{fe} (ω_{eg}) is the $|e\rangle \leftrightarrow |f\rangle$ ($|g\rangle \leftrightarrow |e\rangle$) transition frequency of the qutrit, while ω_a (ω_b) is the frequency of resonator a (b).

Under the large-detuning conditions $|\delta_a| \gg g$ and $|\delta_b| \gg \mu$, the Hamiltonian (1) becomes [46]

$$\begin{aligned} H_e = & -\lambda_a(\hat{a}^+ \hat{a} |g\rangle\langle g| - \hat{a} \hat{a}^+ |e\rangle\langle e|) \\ & -\lambda_b(\hat{b}^+ \hat{b} |e\rangle\langle e| - \hat{b} \hat{b}^+ |f\rangle\langle f|) \\ & + \lambda(e^{-i\Delta t} \hat{a}^+ \hat{b}^+ \sigma_{fg}^- + h.c.), \end{aligned} \quad (2)$$

where $\lambda_a = g^2/\delta_a$, $\lambda_b = \mu^2/\delta_b$, $\lambda = (g\mu/2)(1/|\delta_a| + 1/|\delta_b|)$, $\Delta = |\delta_b| - |\delta_a|$, and $\sigma_{fg}^- = |g\rangle\langle f|$. The first four terms of Eq.(2) describe the photon-number dependent stark shifts of the energy levels $|g\rangle$, $|e\rangle$ and $|f\rangle$, while the last two terms describe the $|f\rangle \leftrightarrow |g\rangle$ coupling caused

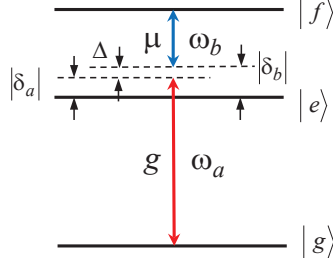


FIG. 2: (Color online) Resonator a is far-off resonant with the $|g\rangle \leftrightarrow |e\rangle$ transition of the qutrit with coupling strength g and detuning $|\delta_a|$, while resonator b is far-off resonant with the $|e\rangle \leftrightarrow |f\rangle$ transition of the qutrit with coupling strength μ and detuning $|\delta_b|$. Here, $|\delta_a| = \omega_a - \omega_{eg}$, $|\delta_b| = \omega_{fe} - \omega_b$, with ω_{eg} (ω_{fe}) being the $|g\rangle \leftrightarrow |e\rangle$ ($|e\rangle \leftrightarrow |f\rangle$) transition frequency of the qutrit, while ω_a (ω_b) being the frequency of resonator a (b). In addition, $\Delta = |\delta_b| - |\delta_a|$. Note that the red vertical line represents the frequency ω_a of resonator a while the blue vertical line represents the frequency ω_b of resonator b .

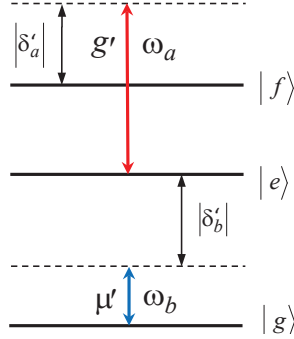


FIG. 3: (Color online) Illustration of resonator a (b) is highly detuned (decoupled) from the $|e\rangle \leftrightarrow |f\rangle$ ($|g\rangle \leftrightarrow |e\rangle$) transition of the qutrit. The high detuning (or decoupling) can be made by prior adjustment of the level spacings of the transmon qutrit or/and the frequency of resonator a (b), such that $|\delta'_a| \gg g'$ and $|\delta'_b| \gg \mu'$. Here, g' is the coupling constant between resonator a and the $|e\rangle \leftrightarrow |f\rangle$ transition, μ' is the coupling constant between resonator b and the $|g\rangle \leftrightarrow |e\rangle$ transition, $|\delta'_a| = \omega_a - \omega_{fe}$ is the detuning between the frequency of resonator a and the $|e\rangle \leftrightarrow |f\rangle$ transition frequency, and $|\delta'_b| = \omega_{eg} - \omega_b$ is the detuning between the frequency of resonator b and the $|g\rangle \leftrightarrow |e\rangle$ transition frequency. Note that the coupling of both resonators with the $|g\rangle \leftrightarrow |f\rangle$ transition of the qutrit is negligible because of the forbidden or very weak $|g\rangle \leftrightarrow |f\rangle$ transition [49,50].

due to the two-resonator cooperation. For $|\Delta| \gg \{\lambda_a, \lambda_b, \lambda\}$, the effective Hamiltonian H_e changes to [51]

$$\begin{aligned} H_e = & -\lambda_a(\hat{a}^+\hat{a}|g\rangle\langle g| - \hat{a}\hat{a}^+|e\rangle\langle e|) \\ & -\lambda_b(\hat{b}^+\hat{b}|e\rangle\langle e| - \hat{b}\hat{b}^+|f\rangle\langle f|) \\ & +\chi(\hat{a}\hat{a}^+\hat{b}\hat{b}^+|f\rangle\langle f| - \hat{a}^+\hat{a}\hat{b}^+\hat{b}|g\rangle\langle g|), \end{aligned} \quad (3)$$

where $\chi = \lambda^2/\Delta$. From Eq. (3) one can see that each term is associated with the level $|g\rangle$, $|e\rangle$, or $|f\rangle$. When the levels $|e\rangle$ and $|f\rangle$ are not occupied, they will remain unpopulated under the Hamiltonian (3). In this case, the effective Hamiltonian (3) reduces to

$$H_e = H_0 + H_{\text{int}}, \quad (4)$$

with

$$\begin{aligned} H_0 &= -\lambda_a\hat{a}^+\hat{a}|g\rangle\langle g| = -\lambda_a\hat{n}_a|g\rangle\langle g|, \\ H_{\text{int}} &= -\chi\hat{a}^+\hat{a}\hat{b}^+\hat{b}|g\rangle\langle g| = -\chi\hat{n}_a\hat{n}_b|g\rangle\langle g|, \end{aligned} \quad (5)$$

where $\hat{n}_a = \hat{a}^+\hat{a}$ ($\hat{n}_b = \hat{b}^+\hat{b}$) is the photon number operator for resonator a (b). Because of $[H_0, H_{\text{int}}] = 0$, the unitary operator $U_1 = e^{-iH_e t}$ can be written as

$$U_1 = e^{-iH_0 t} e^{-iH_{\text{int}} t} = \exp(i\lambda_a\hat{n}_a|g\rangle\langle g|t) \exp(i\chi\hat{n}_a\hat{n}_b|g\rangle\langle g|t). \quad (6)$$

The two logical states $|0\rangle$ and $|1\rangle$ of a cat-state qubit are encoded with cat states of a resonator, i.e., $|0\rangle = M_\alpha^+(|\alpha\rangle + |-\alpha\rangle)$ and $|1\rangle = M_\alpha^-(|\alpha\rangle - |-\alpha\rangle)$, respectively. Here, $M_\alpha^\pm = 1/\sqrt{2(1 \pm e^{-2|\alpha|^2})}$ are normalization coefficients. In terms of $|\alpha\rangle = e^{-|\alpha|^2/2} \sum_{n=0}^{\infty} \frac{\alpha^n}{\sqrt{n!}} |n\rangle$ and $|-\alpha\rangle = e^{-|\alpha|^2/2} \sum_{n=0}^{\infty} \frac{(-\alpha)^n}{\sqrt{n!}} |n\rangle$, we have

$$|0\rangle = \sum_{m=0}^{\infty} C_{2m} |2m\rangle, \quad |1\rangle = \sum_{n=0}^{\infty} C_{2n+1} |2n+1\rangle, \quad (7)$$

where $C_{2m} = 2M_\alpha^+ e^{-|\alpha|^2/2} \alpha^{2m} / \sqrt{(2m)!}$ and $C_{2n+1} = 2M_\alpha^- e^{-|\alpha|^2/2} \alpha^{2n+1} / \sqrt{(2n+1)!}$. From Eq. (7), one can see that the state $|0\rangle$ is orthogonal to the state $|1\rangle$, which is independent of α (except for $\alpha = 0$).

The four logical states of two cat-state qubits are $|00\rangle_{ab}$, $|01\rangle_{ab}$, $|10\rangle_{ab}$ and $|11\rangle_{ab}$, where the left 0 and 1 are encoded with cat states of resonator a while the right 0 and 1 are

encoded with cat states of resonator b . Suppose that the qutrit is initially in the ground state $|g\rangle$. For an interaction time $t = t_1$, the unitary operation U_1 leads to the following state transformations (see Appendix for details)

$$\begin{aligned}
U_1|00\rangle_{ab}|g\rangle &= \sum_{m,m'=0}^{\infty} F_1(m, m', t_1) C_{2m} C_{2m'} |2m\rangle_a |2m'\rangle_b |g\rangle, \\
U_1|01\rangle_{ab}|g\rangle &= \sum_{m,n'=0}^{\infty} F_2(m, n', t_1) C_{2m} C_{2n'+1} |2m\rangle_a |2n'+1\rangle_b |g\rangle, \\
U_1|10\rangle_{ab}|g\rangle &= \sum_{n,m'=0}^{\infty} F_3(n, m', t_1) C_{2n+1} C_{2m'} |2n+1\rangle_a |2m'\rangle_b |g\rangle, \\
U_1|11\rangle_{ab}|g\rangle &= \sum_{n,n'=0}^{\infty} F_4(n, n', t_1) C_{2n+1} C_{2n'+1} |2n+1\rangle_a |2n'+1\rangle_b |g\rangle,
\end{aligned} \tag{8}$$

with

$$\begin{aligned}
F_1(m, m', t_1) &= \exp(i\lambda_a 2mt_1) \exp[i(2m)(2m')\chi t_1], \\
F_2(m, n', t_1) &= \exp(i\lambda_a 2mt_1) \exp[i(2m)(2n'+1)\chi t_1], \\
F_3(n, m', t_1) &= \exp[i\lambda_a (2n+1)t_1] \exp[i(2n+1)(2m')\chi t_1], \\
F_4(n, n', t_1) &= \exp[i\lambda_a (2n+1)t_1] \exp[i(2n+1)(2n'+1)\chi t_1].
\end{aligned} \tag{9}$$

We now adjust the frequency of resonator a such that resonator a is far-off resonant with the $|g\rangle \leftrightarrow |e\rangle$ transition of the qutrit with coupling strength \tilde{g} and detuning $|\tilde{\delta}_a|$ (Fig. 4), while it is highly detuned (decoupled) from the $|e\rangle \leftrightarrow |f\rangle$ transition (Fig. 5). Here, $|\tilde{\delta}_a| = \omega_{eg} - \tilde{\omega}_a$ (Fig. 4), with $\tilde{\omega}_a$ being the adjusted frequency of resonator a . In addition, adjust the frequency of resonator b such that resonator b is decoupled from the qutrit. Note that the frequency of a microwave resonator can be rapidly adjusted with a few nanoseconds [52,53]. Under these considerations, the Hamiltonian in the interaction picture and after making the RWA is given by

$$H_{I,2} = \tilde{g}(e^{i\tilde{\delta}_a t} \hat{a} \sigma_{eg}^+ + h.c.), \tag{10}$$

where $\tilde{\delta}_a = |\tilde{\delta}_a| = \omega_{eg} - \tilde{\omega}_a > 0$.

For $\tilde{\delta}_a \gg \tilde{g}$ and the level $|e\rangle$ being not occupied, we have

$$\tilde{H}_e = -\tilde{\lambda}_a \hat{n}_a |g\rangle \langle g|, \tag{11}$$

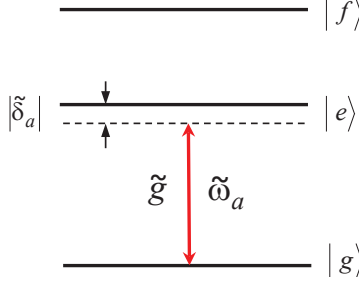


FIG. 4: (Color online) Resonator a is far-off resonant with the $|g\rangle \leftrightarrow |e\rangle$ transition of the qutrit with coupling strength \tilde{g} and detuning $|\tilde{\delta}_a|$. Here, $|\tilde{\delta}_a| = \omega_{eg} - \tilde{\omega}_a$, with $\tilde{\omega}_a$ being the adjusted frequency of resonator a (labelled by the vertical line). The frequency of resonator b is adjusted such that resonator b is decoupled from the qutrit. Note that the dispersive qutrit-cavity coupling with a detuning $|\tilde{\delta}_a|$ illustrated here can also be obtained by adjusting the level spacings of the qutrit but the cavity frequency being fixed.

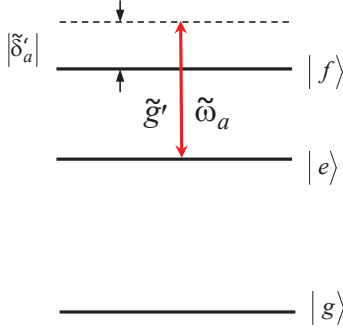


FIG. 5: (Color online) Illustration of resonator a is highly detuned (decoupled) from the $|e\rangle \leftrightarrow |f\rangle$ transition of the qutrit. The decoupling can be made as long as the condition $|\tilde{\delta}'_a| \gg \tilde{g}'$ can be satisfied. Here, \tilde{g}' is the coupling constant between resonator a and the $|e\rangle \leftrightarrow |f\rangle$ transition, while $|\tilde{\delta}'_a| = \tilde{\omega}_a - \omega_{fe}$ is the detuning between the frequency of resonator a and the $|e\rangle \leftrightarrow |f\rangle$ transition frequency. Note that the coupling of resonator a with the $|g\rangle \leftrightarrow |f\rangle$ transition of the qutrit is negligible because of the forbidden or very weak $|g\rangle \leftrightarrow |f\rangle$ transition [49,50]. In addition, since the frequency of resonator b is far detuned, resonator b is decoupled from the qutrit.

with $\tilde{\lambda}_a = \tilde{g}^2/\tilde{\delta}_a$. Then, performing a unitary transformation $U_2 = \exp(i\tilde{\lambda}_a \hat{n}_a |g\rangle\langle g| t_2)$ for an

interaction time $t = t_2$, we obtain from Eqs. (8) and (9)

$$\begin{aligned}
U_2 U_1 |00\rangle_{ab} |g\rangle &= \sum_{m,m'=0}^{\infty} \tilde{F}_1(m, m', t_1) C_{2m} C_{2m'} |2m\rangle_a |2m'\rangle_b |g\rangle, \\
U_2 U_1 |01\rangle_{ab} |g\rangle &= \sum_{m,n'=0}^{\infty} \tilde{F}_2(m, n', t_1) C_{2m} C_{2n'+1} |2m\rangle_a |2n'+1\rangle_b |g\rangle, \\
U_2 U_1 |10\rangle_{ab} |g\rangle &= \sum_{n,m'=0}^{\infty} \tilde{F}_3(n, m', t_1) C_{2n+1} C_{2m'} |2n+1\rangle_a |2m'\rangle_b |g\rangle, \\
U_2 U_1 |11\rangle_{ab} |g\rangle &= \sum_{n,n'=0}^{\infty} \tilde{F}_4(n, n', t_1) C_{2n+1} C_{2n'+1} |2n+1\rangle_a |2n'+1\rangle_b |g\rangle.
\end{aligned} \tag{12}$$

with

$$\begin{aligned}
\tilde{F}_1(m, m', t_1) &= \exp[i2m(\lambda_a t_1 + \tilde{\lambda}_a t_2)] \exp[i(2m)(2m')\chi t_1], \\
\tilde{F}_2(m, n', t_1) &= \exp[i2m(\lambda_a t_1 + \tilde{\lambda}_a t_2)] \exp[i(2m)(2n+1)\chi t_1], \\
\tilde{F}_3(n, m', t_1) &= \exp[i(2n+1)(\lambda_a t_1 + \tilde{\lambda}_a t_2)] \exp[i(2n+1)(2m')\chi t_1], \\
\tilde{F}_4(n, n', t_1) &= \exp[i(2n+1)(\lambda_a t_1 + \tilde{\lambda}_a t_2)] \exp[i(2n+1)(2n'+1)\chi t_1].
\end{aligned} \tag{13}$$

Note that the index factors $(2m)(2m')$, $(2m)(2n+1)$, and $(2n+1)(2m')$ of Eq. (13) are even numbers, while the index factor $(2n+1)(2n'+1)$ is an odd number. By setting $\lambda_a = -\tilde{\lambda}_a$ (i.e., $g^2/\delta_a = -\tilde{g}^2/\tilde{\delta}_a$) and $t_2 = t_1 = \pi/|\chi|$, we have $\tilde{F}_1(m, m', t_1) = \tilde{F}_2(m, n', t_1) = \tilde{F}_3(n, m', t_1) = 1$ but $\tilde{F}_4(n, n', t_1) = -1$. Hence, the states (12) become

$$\begin{aligned}
U_2 U_1 |00\rangle_{ab} |g\rangle &= |00\rangle_{ab} |g\rangle, \\
U_2 U_1 |01\rangle_{ab} |g\rangle &= |01\rangle_{ab} |g\rangle, \\
U_2 U_1 |10\rangle_{ab} |g\rangle &= |10\rangle_{ab} |g\rangle, \\
U_2 U_1 |11\rangle_{ab} |g\rangle &= -|11\rangle_{ab} |g\rangle,
\end{aligned} \tag{14}$$

which shows that the above two basic operations (i.e., U_1 and U_2) have completed a universal controlled-phase gate of two cat-state qubits, described by $|00\rangle_{ab} \rightarrow |00\rangle_{ab}$, $|01\rangle_{ab} \rightarrow |01\rangle_{ab}$, $|10\rangle_{ab} \rightarrow |10\rangle_{ab}$, and $|11\rangle_{ab} \rightarrow -|11\rangle_{ab}$. After this gate, an arbitrary pure state of two cat-state qubits, given by $|\phi\rangle_{ab} = \alpha|00\rangle_{ab} + \beta|01\rangle_{ab} + \gamma|10\rangle_{ab} + \zeta|11\rangle_{ab}$, is transformed as follows

$$|\phi\rangle_{ab} \rightarrow \alpha|00\rangle_{ab} + \beta|01\rangle_{ab} + \gamma|10\rangle_{ab} - \zeta|11\rangle_{ab}. \tag{15}$$

From description given above, one can see that the qutrit remains in the ground state during the entire operation. Hence, decoherence from the qutrit is greatly suppressed.

As shown above, the Hamiltonian (11) for the second unitary operation (U_2) was constructed by tuning cavity frequency. However, we point out that tuning cavity frequency is unnecessary. Alternatively, one can obtain the Hamiltonian (11) by adjusting the level spacings of the qutrit to meet the conditions required for constructing this Hamiltonian (11). Note that for a SC qutrit, the level spacings can be rapidly (within 1-3 ns) adjusted by varying external control parameters (e.g., magnetic flux applied to the superconducting loop of a SC phase, transmon [54], Xmon [10], or flux qubit/qutrit [55]).

We should mention that the Hamiltonian (4) was previously proposed to realize a controlled-phase gate of two *discrete-variable* qubits [56], for which the two logic states of a qubit are encoded with *the vacuum state and a single-photon state* of a cavity mode. In stark contrast, the present work aims at implementing a controlled-phase gate of two *continuous-variable* qubits, for which the two logic states of a qubit are encoded with *cat states* of a resonator or cavity.

III. POSSIBLE EXPERIMENTAL IMPLEMENTATION

In above, we have explicitly shown how to realize a controlled-phase gate of two cat-state qubits. We now give a brief discussion on the experimental feasibility by considering a setup of a SC transmon qutrit coupled to two 3D microwave resonators or cavities.

From the description given above, one can see that the gate implementation involves the following two basic operations:

(i) The first operation is described by the Hamiltonian (1). In reality, the inter-resonator crosstalk between the two resonators is inevitable [57], and there exist the unwanted coupling of resonator a with the $|e\rangle \leftrightarrow |f\rangle$ transition and the unwanted coupling of resonator b with the $|g\rangle \leftrightarrow |e\rangle$ transition of the qutrit. When these factors are taken into account, the Hamiltonian (1) becomes

$$\begin{aligned}\tilde{H}_{1,1} = & g(e^{i\delta_a t}\hat{a}\sigma_{eg}^+ + h.c.) + \mu(e^{i\delta_b t}\hat{b}\sigma_{fe}^+ + h.c.) \\ & + g'(e^{i\delta'_a t}\hat{a}\sigma_{fe}^+ + h.c.) + \mu'(e^{i\delta'_b t}\hat{b}\sigma_{eg}^+ + h.c.) \\ & + g_{ab}(e^{-i\Delta_{ab} t}\hat{a}\hat{b}^+ + h.c.),\end{aligned}\tag{16}$$

where the first bracket term represents the interaction of resonator a with the $|g\rangle \leftrightarrow |e\rangle$ transition, the second bracket term represents the interaction of resonator b with the $|e\rangle \leftrightarrow |f\rangle$ transition, the third bracket term represents the unwanted coupling between resonator a and the $|e\rangle \leftrightarrow |f\rangle$ transition with coupling strength g' and detuning $\delta'_a = \omega_{fe} - \omega_a < 0$ (Fig. 3), and the fourth bracket term represents the unwanted coupling between resonator b and the $|g\rangle \leftrightarrow |e\rangle$ transition of the qutrit with coupling strength μ' and detuning $\delta'_b = \omega_{eg} - \omega_b > 0$ (Fig. 3). In addition, the last bracket term of Eq. (16) represents the inter-resonator crosstalk, where g_{ab} is the coupling strength between the two resonators while $\Delta_{ab} = \omega_a - \omega_b$ is the difference between the two-resonator frequencies.

(ii) The second operation is described by the Hamiltonian (10). In practice, the inter-resonator crosstalk between the two resonators and the unwanted coupling of resonator a with the $|e\rangle \leftrightarrow |f\rangle$ transition should be considered. Note that for the second operation, the frequency of resonator b was far detuned such that resonator b is decoupled from the qutrit. When these factors are taken into account, the Hamiltonian (10) becomes

$$\begin{aligned} \tilde{H}_{1,2} = & \tilde{g}(e^{i\tilde{\delta}_a t} \hat{a} \sigma_{eg}^+ + h.c.) + \tilde{g}'(e^{i\tilde{\delta}'_a t} \hat{a} \sigma_{fe}^+ + h.c.) \\ & + \tilde{g}_{ab}(e^{-i\tilde{\Delta}_{ab} t} \hat{a} \hat{b}^+ + h.c.), \end{aligned} \quad (17)$$

where the first bracket term represents the interaction of resonator a with the $|g\rangle \leftrightarrow |e\rangle$ transition, while the second bracket term represents the unwanted coupling between resonator a and the $|e\rangle \leftrightarrow |f\rangle$ transition with coupling strength \tilde{g}' and detuning $\tilde{\delta}'_a = \omega_{fe} - \tilde{\omega}_a < 0$ (Fig. 5). The last bracket term of Eq. (17) represents the inter-resonator crosstalk, where \tilde{g}_{ab} is the coupling strength between the two resonators while $\tilde{\Delta}_{ab} = \tilde{\omega}_a - \tilde{\omega}_b$ is the difference between the two-resonator frequencies.

The dynamics of the lossy system is determined by

$$\begin{aligned} \frac{d\rho}{dt} = & -i[\tilde{H}_{1,i}, \rho] + \kappa_a \mathcal{L}[a] + \kappa_b \mathcal{L}[b] \\ & + \gamma_{eg} \mathcal{L}[\sigma_{eg}^-] + \gamma_{fe} \mathcal{L}[\sigma_{fe}^-] + \gamma_{fg} \mathcal{L}[\sigma_{fg}^-] \\ & + \sum_{j=e,f} \{ \gamma_{\varphi j} (\sigma_{jj} \rho \sigma_{jj} - \sigma_{jj} \rho / 2 - \rho \sigma_{jj} / 2) \}, \end{aligned} \quad (18)$$

where $\tilde{H}_{1,i}$ is the full Hamiltonian given above ($i = 1, 2$), $\sigma_{eg}^- = |g\rangle\langle e|$, $\sigma_{fe}^- = |e\rangle\langle f|$, $\sigma_{fg}^- = |g\rangle\langle f|$, $\sigma_{jj} = |j\rangle\langle j|$ ($j = e, f$); and $\mathcal{L}[\xi] = \xi \rho \xi^\dagger - \xi^\dagger \xi \rho / 2 - \rho \xi^\dagger \xi / 2$, with

$\xi = a, b, \sigma_{eg}^-, \sigma_{fe}^-, \sigma_{fg}^-$. Here, $\kappa_a(\kappa_b)$ is the photon decay rate of resonator a (b). In addition, γ_{eg} is the energy relaxation rate for the level $|e\rangle$ of the qutrit, $\gamma_{fe}(\gamma_{fg})$ is the energy relaxation rate of the level $|f\rangle$ of the qutrit for the decay path $|f\rangle \longrightarrow |e\rangle(|g\rangle)$, and $\gamma_{\varphi j}$ is the dephasing rate of the level $|j\rangle$ ($j = e, f$) of the qutrit.

The fidelity of the operations is given by

$$\mathcal{F} = \sqrt{\langle \psi_{\text{id}} | \rho | \psi_{\text{id}} \rangle}, \quad (19)$$

where $|\psi_{\text{id}}\rangle$ is the output state of an ideal system without dissipation, dephasing and crosstalk *etc.*; while ρ is the final practical density operator of the system when the operation is performed in a realistic situation. For simplicity, choose $\alpha = \cos \theta \cos \varphi$, $\beta = \cos \theta \sin \varphi$, $\gamma = \sin \theta \cos \varphi$, and $\zeta = \sin \theta \sin \varphi$, which satisfy the normalization condition $|\alpha|^2 + |\beta|^2 + |\gamma|^2 + |\zeta|^2 = 1$. The initial state of the qutrit-resonator system is thus written as $|\psi_{\text{in}}\rangle = (\cos \theta \cos \varphi |00\rangle_{ab} + \cos \theta \sin \varphi |01\rangle_{ab} + \sin \theta \cos \varphi |10\rangle_{ab} + \sin \theta \sin \varphi |11\rangle_{ab}) |g\rangle$. The output state is $|\psi_{\text{id}}\rangle = (\cos \theta \cos \varphi |00\rangle_{ab} + \cos \theta \sin \varphi |01\rangle_{ab} + \sin \theta \cos \varphi |10\rangle_{ab} - \sin \theta \sin \varphi |11\rangle_{ab}) |g\rangle$. In the following, we will consider the cases: (i) $\theta = \varphi = \pi/4$; (ii) $\theta = \varphi = \pi/3$; (iii) $\theta = \pi/4, \varphi = \pi/3$; and (iv) $\theta = \pi/3, \varphi = \pi/4$; which correspond to four initial states.

For a transmon qutrit, the typical transition frequency between two neighboring levels can be varied from 3 to 10 GHz. In addition, the anharmonicity of the level spacings for a transmon qutrit can be made to be within 100 ~ 500 MHz [14]. As an example, we thus consider $\omega_{eg}/2\pi = 6.5$ GHz and $\omega_{fe}/2\pi = 6$ GHz. By choosing $\delta_a/2\pi = -1.0$ GHz and $\delta_b/2\pi = 1.1$ GHz, we have $\omega_a/2\pi = 7.5$ GHz and $\omega_b/2\pi = 4.9$ GHz, for which we have $\Delta_{ab}/2\pi = 2.6$ GHz. We set $\tilde{\delta}_a/2\pi = 1.0$ GHz, for which we have $\tilde{\omega}_a/2\pi = 5.5$ GHz. By choosing $\tilde{\omega}_b/2\pi = 3.5$ GHz, we have $\tilde{\Delta}_{ab}/2\pi = 2$ GHz. In addition, we have $\delta'_a/2\pi = -1.5$ GHz, $\delta'_b/2\pi = 1.6$ GHz, and $\tilde{\delta}'_a/2\pi = -0.5$ GHz. Other parameters used in the numerical simulation are: (i) $\gamma_{eg}^{-1} = 60 \mu\text{s}$, $\gamma_{fg}^{-1} = 150 \mu\text{s}$ [58], $\gamma_{fe}^{-1} = 30 \mu\text{s}$, $\gamma_{\phi e}^{-1} = \gamma_{\phi f}^{-1} = 20 \mu\text{s}$, (ii) $g/2\pi = \mu/2\pi = 95$ MHz (available in experiments [14]), and (iii) $\alpha = 0.5$. Here, we consider a rather conservative case for decoherence time of transmon qutrits because energy relaxation time with a range from 65 μs to 0.1 ms and dephasing time from 25 μs to 70 μs have been experimentally reported for a 3D superconducting transmon device [7,11,48]. The value of \tilde{g} is determined according to $g^2/\delta_a = -\tilde{g}^2/\tilde{\delta}_a$, given g , δ_a , and $\tilde{\delta}_a$. For a transmon qutrit [49], one has $g' \sim \sqrt{2}g$, $\mu' \sim \mu/\sqrt{2}$, and $\tilde{g}' \sim \sqrt{2}\tilde{g}$. We set $g_{ab} = 0.01g$, which can be

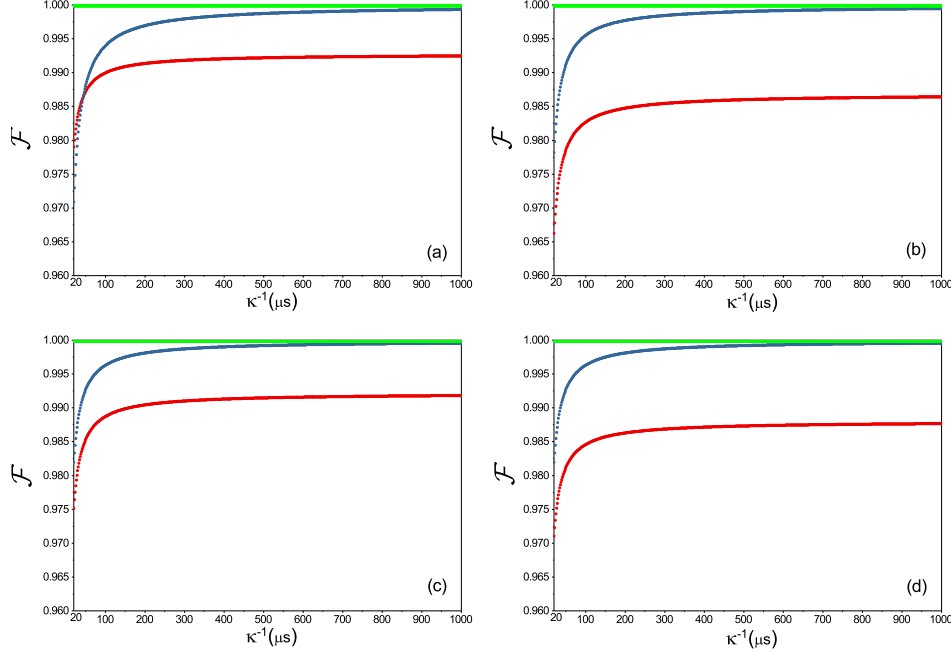


FIG. 6: (Color online) Fidelity versus κ^{-1} . The plots are drawn for $\alpha = 0.5$. Other parameters used in the numerical simulation are referred to the text. Green curves are based on the effective Hamiltonians (4) and (11) but not considering decoherence and the inter-resonator crosstalk; blue curves are based on the effective Hamiltonians (4) and (11) and considering decoherence and the inter-resonator crosstalk; while red curves are based on the full Hamiltonians (16) and (17) and taking decoherence and the inter-resonator crosstalk into account. (a) is plotted for $\theta = \varphi = \pi/4$; (b) is for $\theta = \varphi = \pi/3$; (c) is for $\theta = \pi/4, \varphi = \pi/3$; while (d) is for $\theta = \pi/3, \varphi = \pi/4$.

readily achieved in experiments [33].

For simplicity, assume $\kappa_a = \kappa_b = \kappa$. By solving the master equation (18), we numerically calculate the fidelity versus κ^{-1} , as shown in Fig. 6. Fig. 6(a) is plotted for $\theta = \varphi = \pi/4$. Fig. 6(b) is for $\theta = \varphi = \pi/3$. Fig. 6(c) is for $\theta = \pi/4, \varphi = \pi/3$. Fig. 6(d) is for $\theta = \pi/3, \varphi = \pi/4$. The red curves in Fig. 6 are drawn by numerical simulations, which are based on the full Hamiltonians $\tilde{H}_{I,1}$ in Eq. (16) and $\tilde{H}_{I,2}$ in Eq. (17) and take decoherence and the inter-resonator crosstalk into account. The red curves illustrate that when $\kappa^{-1} \geq 300 \mu$, fidelity exceeds: (i) 0.9918 for $\theta = \varphi = \pi/4$; (ii) 0.9854 for $\theta = \varphi = \pi/3$; (iii) 0.9910 for $\theta = \pi/4, \varphi = \pi/3$; and (iv) 0.9868 for $\theta = \pi/3, \varphi = \pi/4$. These results imply that the fidelity depends on the choice of the initial state of the two resonators and a high fidelity can be obtained when the gate is performed in a realistic situation.

To see how good the approximations are, we have calculated the fidelity based on the effective Hamiltonians given in Eq. (4) and Eq. (11) and by considering decoherence and the inter-resonator crosstalk (see the blue curves in Fig. 6). From the red curves and the blue curves depicted in Fig. 6, one can see that compared to the case of the gate being performed based on the effective Hamiltonians, the fidelity for the gate performed in a realistic situation is slightly decreased by 0.9%–1.5%. This implies that the approximations made for the effective Hamiltonians are reasonable.

Lifetime ~ 1 ms of microwave photons has been experimentally demonstrated in a coaxial resonator [17,48]. For $\kappa^{-1} = 300 \mu\text{s}$, we have $Q_a = 1.2 \times 10^7$ for $\omega_a/2\pi = 6.5$ GHz, $\tilde{Q}_a = 1.0 \times 10^7$ for $\tilde{\omega}_a/2\pi = 5.5$ GHz, $Q_b = 9.2 \times 10^6$ for $\omega_b/2\pi = 4.9$ GHz, and $\tilde{Q}_b = 6.6 \times 10^6$ for $\tilde{\omega}_b/2\pi = 3.5$ GHz. Note that a high quality factor $Q = 3.5 \times 10^7$ of a 3D superconducting resonator has been experimentally demonstrated [17]. The analysis here implies that the high-fidelity implementation of the proposed gate is feasible within the current circuit QED technology.

IV. CONCLUSIONS

We have proposed a method to realize a universal controlled-phase gate of two cat-state qubits, via two microwave resonators coupled to a superconducting transmon qutrit. This method can be extended to a wide range of physical systems such as two microwave or optical cavities coupled to a single three-level natural or artificial atom. As shown above, this proposal has these features. During the gate operation, the qutrit remains in the ground state; thus decoherence from the qutrit is greatly suppressed. Because only two basic operations are needed and neither classical pulse nor measurement is required, the gate realization is simple. Our numerical simulations show that high-fidelity implementation of the proposed gate is feasible with current circuit QED technology. To the best of our knowledge, this work is the first to demonstrate the implementation of a controlled-phase gate with cat-state qubits based on cavity- or circuit-QED. We hope that this work will stimulate experimental activities in the near future.

ACKNOWLEDGMENTS

This work was supported by Ministry of Science and Technology of China (No. 2016YFA0301802); National Natural Science Foundation of China (11504075, 11074062,

11247008, 11374083); Zhejiang Natural Science Foundation (LZ13A040002); Hangzhou-City Quantum Information and Quantum Optics Innovation Research Team; The open project funding from CAS Key Laboratory of Quantum Information, University of Science and Technology of China (project number KQI201710).

APPENDIX

Under the unitary operation U_1 and for an interaction time $t = t_1$, the state transformations for the four logical states $|00\rangle_{ab}$, $|01\rangle_{ab}$, $|10\rangle_{ab}$ and $|11\rangle_{ab}$ of the two cat-state qubits are listed below in details.

$$\begin{aligned}
& U_1|00\rangle_{ab}|g\rangle \\
&= \exp(i\lambda_a\hat{n}_a|g\rangle\langle g|t_1) \exp(i\chi\hat{n}_a\hat{n}_b|g\rangle\langle g|t_1) \sum_{m=0}^{\infty} C_{2m}|2m\rangle_a \sum_{m'=0}^{\infty} C_{2m'}|2m'\rangle_b|g\rangle \\
&= \exp(i\lambda_a\hat{n}_a|g\rangle\langle g|t_1) \exp(i\chi\hat{n}_a\hat{n}_b|g\rangle\langle g|t_1) \sum_{m=0}^{\infty} \sum_{m'=0}^{\infty} C_{2m}C_{2m'}|2m\rangle_a|2m'\rangle_b|g\rangle \\
&= \exp(i\lambda_a\hat{n}_at_1) \exp(i\chi\hat{n}_a\hat{n}_bt_1) \sum_{m=0}^{\infty} \sum_{m'=0}^{\infty} C_{2m}C_{2m'}|2m\rangle_a|2m'\rangle_b|g\rangle \\
&= \sum_{m=0}^{\infty} \sum_{m'=0}^{\infty} C_{2m}C_{2m'} \exp(i\lambda_a\hat{n}_at_1) \exp(i\chi\hat{n}_a\hat{n}_bt_1)|2m\rangle_a|2m'\rangle_b|g\rangle \\
&= \sum_{m,m'=0}^{\infty} F_1(m, m', t_1) C_{2m}C_{2m'}|2m\rangle_a|2m'\rangle_b|g\rangle, \tag{20}
\end{aligned}$$

$$\begin{aligned}
& U_1|01\rangle_{ab}|g\rangle \\
&= \exp(i\lambda_a\hat{n}_a|g\rangle\langle g|t_1) \exp(i\chi\hat{n}_a\hat{n}_b|g\rangle\langle g|t_1) \sum_{m=0}^{\infty} C_{2m}|2m\rangle_a \sum_{n'=0}^{\infty} C_{2n'+1}|2n'+1\rangle_b|g\rangle \\
&= \exp(i\lambda_a\hat{n}_a|g\rangle\langle g|t_1) \exp(i\chi\hat{n}_a\hat{n}_b|g\rangle\langle g|t_1) \sum_{m=0}^{\infty} \sum_{n'=0}^{\infty} C_{2m}C_{2n'+1}|2m\rangle_a|2n'+1\rangle_b|g\rangle \\
&= \exp(i\lambda_a\hat{n}_at_1) \exp(i\chi\hat{n}_a\hat{n}_bt_1) \sum_{m=0}^{\infty} \sum_{n'=0}^{\infty} C_{2m}C_{2n'+1}|2m\rangle_a|2n'+1\rangle_b|g\rangle \\
&= \sum_{m=0}^{\infty} \sum_{n'=0}^{\infty} C_{2m}C_{2n'+1} \exp(i\lambda_a\hat{n}_at_1) \exp(i\chi\hat{n}_a\hat{n}_bt_1)|2m\rangle_a|2n'+1\rangle_b|g\rangle \\
&= \sum_{m,n'=0}^{\infty} F_2(m, n', t_1) C_{2m}C_{2n'+1}|2m\rangle_a|2n'+1\rangle_b|g\rangle, \tag{21}
\end{aligned}$$

with

$$\begin{aligned} F_1(m, m', t_1) &= \exp(i\lambda_a 2mt_1) \exp[i(2m)(2m')\chi t_1], \\ F_2(m, n', t_1) &= \exp(i\lambda_a 2mt_1) \exp[i(2m)(2n' + 1)\chi t_1]. \end{aligned} \quad (22)$$

Similarly, one can easily find that

$$\begin{aligned} U_1|10\rangle_{ab}|g\rangle &= \exp(i\lambda_a \hat{n}_a |g\rangle\langle g| t_1) \exp(i\chi \hat{n}_a \hat{n}_b |g\rangle\langle g| t_1) \otimes \\ &\quad \sum_{n=0}^{\infty} C_{2n+1} |2n+1\rangle_a \sum_{m'=0}^{\infty} C_{2m'} |2m'\rangle_b |g\rangle \\ &= \sum_{n, m'=0}^{\infty} F_3(n, m', t_1) C_{2n+1} C_{2m'} |2n+1\rangle_a |2m'\rangle_b |g\rangle, \end{aligned} \quad (23)$$

$$\begin{aligned} U_1|11\rangle_{ab}|g\rangle &= \exp(i\lambda_a \hat{n}_a |g\rangle\langle g| t_1) \exp(i\chi \hat{n}_a \hat{n}_b |g\rangle\langle g| t_1) \otimes \\ &\quad \sum_n^{\infty} C_{2n+1} |2n+1\rangle_a \otimes \sum_{n'=0}^{\infty} C_{2n'+1} |2n'+1\rangle_b |g\rangle \\ &= \sum_{n, n'=0}^{\infty} F_4(n, n', t_1) C_{2n+1} C_{2n'+1} |2n+1\rangle_a |2n'+1\rangle_b |g\rangle, \end{aligned} \quad (24)$$

with

$$\begin{aligned} F_3(n, m', t_1) &= \exp[i\lambda_a (2n+1)t_1] \exp[i(2n+1)(2m')\chi t_1], \\ F_4(n, n', t_1) &= \exp[i\lambda_a (2n+1)t_1] \exp[i(2n+1)(2n'+1)\chi t_1]. \end{aligned} \quad (25)$$

-
- [1] J. Clarke and F. K. Wilhelm, Superconducting quantum bits, *Nature* **453**, 1031 (2008).
 - [2] I. Buluta, S. Ashhab, and F. Nori, Natural and artificial atoms for quantum computation, *Rep. Prog. Phys.* **74**, 104401 (2011).
 - [3] J. Q. You and F. Nori, Atomic physics and quantum optics using superconducting circuits, *Nature* **474**, 589 (2011).
 - [4] Z. L. Xiang, S. Ashhab, J. Q. You, and F. Nori, Hybrid quantum circuits: Superconducting circuits interacting with other quantum systems, *Rev. Mod. Phys.* **85**, 623 (2013).
 - [5] J. Bylander, S. Gustavsson, F. Yan, F. Yoshihara, K. Harrabi, G. F. David, G. Cory, Y. Nakamura, J. S. Tsai, and W. D. Oliver, Noise spectroscopy through dynamical decoupling with a superconducting flux qubit, *Nat. Phys.* **7**, 565 (2011).

- [6] H. Paik, D. I. Schuster, L. S. Bishop, G. Kirchmair, G. Catelani, A. P. Sears, B. R. Johnson, M. J. Reagor, L. Frunzio, and L. I. Glazman, *et al.*, Observation of high coherence in josephson junction qubits measured in a three-dimensional circuit QED architecture, *Phys. Rev. Lett.* **107**, 240501 (2011).
- [7] C. Rigetti, S. Poletto, J. M. Gambetta, B. L. T. Plourde, J. M. Chow, A. D. Corcoles, J. A. Smolin, S. T. Merkel, J. R. Rozen, and G. A. Keefe *et al.*, Superconducting qubit in waveguide cavity with coherence time approaching 0.1 ms, *Phys. Rev. B* **86**, 100506(R) (2012).
- [8] Y. Chen, C. Neill, P. Roushan, N. Leung, M. Fang, R. Barends, J. Kelly, B. Campbell, Z. Chen, and B. Chiaro *et al.*, Qubit architecture with high coherence and fast tunable coupling, *Phys. Rev. Lett.* **113**, 220502 (2014).
- [9] M. Stern, G. Catelani, Y. Kubo, C. Grezes, A. Bienfait, D. Vion, D. Esteve, and P. Bertet, Flux qubits with long coherence times for hybrid quantum circuits, *Phys. Rev. Lett.* **113**, 123601 (2014).
- [10] R. Barends, J. Kelly, A. Megrant, D. Sank, E. Jeffrey, Y. Chen, Y. Yin, B. Chiaro, J. Mutus, and C. Neill *et al.*, Coherent Josephson qubit suitable for scalable quantum integrated circuits, *Phys. Rev. Lett.* **111**, 080502 (2013).
- [11] M. J. Peterer, S. J. Bader, X. Jin, F. Yan, A. Kamal, T. J. Gudmundsen, P. J. Leek, T. P. Orlando, W. D. Oliver, and S. Gustavsson, Coherence and decay of higher energy levels of a superconducting transmon qubit. *Phys. Rev. Lett.* **114**, 010501 (2015).
- [12] F. Yan, S. Gustavsson, A. Kamal, J. Birenbaum, A. P. Sears, D. Hover, T. J. Gudmundsen, J. L. Yoder, T. P. Orlando, and J. Clarke *et al.*, The Flux Qubit Revisited to Enhance Coherence and Reproducibility, *Nat. Commun.* **7**, 12964 (2016).
- [13] A. Wallraff, D. I. Schuster, A. Blais, L. Frunzio, R. S. Huang, J. Majer, S. Kumar, S. M. Girvin and R. J. Schoelkopf, Strong coupling of a single photon to a superconducting qubit using circuit quantum electrodynamics, *Nature* **431**, 162 (2004).
- [14] T. Niemczyk, F. Deppe, H. Huebl, E. P. Menzel, F. Hocke, M. J. Schwarz, J. J. Garcia-Ripoll, D. Zueco, T. Hümmer, and E. Solano *et al.*, Circuit quantum electrodynamics in the ultrastrong-coupling regime. *Nat. Phys.* **6**, 772 (2010).
- [15] W. Chen, D. A. Bennett, V. Patel and J. E. Lukens, Substrate and process dependent losses in superconducting thin film resonators, *Supercond. Sci. Technol.* **21**, 075013 (2008).
- [16] P. J. Leek, M. Baur, J. M. Fink, R. Bianchetti, L. Steffen, S. Filipp, and A. Wallraff, Cavity

- quantum electrodynamics with separate photon storage and qubit readout modes, *Phys. Rev. Lett.* **104**, 100504 (2010).
- [17] M. Reagor, W. Pfaff, C. Axline, R. W. Heeres, N. Ofek, K. Sliwa, E. Holland, C. Wang, J. Blumoff, and K. Chou *et al.*, A quantum memory with near-millisecond coherence in circuit QED, *Phys. Rev. B* **94**, 014506 (2016).
 - [18] C. P. Yang, S. I. Chu, and S. Han, Possible realization of entanglement, logical gates, and quantum-information transfer with superconducting-quantum-interference-device qubits in cavity QED, *Phys. Rev. A* **67**, 042311 (2003).
 - [19] J. Q. You and F. Nori, Quantum information processing with superconducting qubits in a microwave field, *Phys. Rev. B* **68**, 064509 (2003).
 - [20] A. Blais, R. S. Huang, A. Wallraff, S. M. Girvin, and R. J. Schoelkopf, Cavity quantum electrodynamics for superconducting electrical circuits: An architecture for quantum computation, *Phys. Rev. A* **69**, 062320 (2004).
 - [21] M. Hofheinz, H. Wang, M. Ansmann, R. C. Bialczak, E. Lucero, M. Neeley, A. D. O’Connell, D. Sank, J. Wenner, J. M. Martinis, and A. N. Cleland, Synthesizing arbitrary quantum states in a superconducting resonator, *Nature (London)* **459**, 546 (2009).
 - [22] H. Wang, M. Hofheinz, J. Wenner, M. Ansmann, R. C. Bialczak, M. Lenander, E. Lucero, M. Neeley, A. D. O’Connell, D. Sank, M. Weides, A. N. Cleland, and J. M. Martinis, Improving the Coherence Time of Superconducting Coplanar Resonators, *Appl. Phys. Lett.* **95**, 233508 (2009).
 - [23] M. H. Devoret and R. J. Schoelkopf, Superconducting circuits for quantum information: an outlook, *Science* **339**, 1169 (2013).
 - [24] F. Marquardt and C. Bruder, Superposition of two mesoscopically distinct quantum states: Coupling a cooper-pair box to a large superconducting island, *Phys. Rev. B* **63**, 054514 (2001).
 - [25] Y. X. Liu, L. F. Wei, and F. Nori, Generation of nonclassical photon states using a superconducting qubit in a microcavity, *Europhysics Letters* **67**, 941 (2004).
 - [26] K. Moon and S. M. Girvin, Theory of microwave parametric down-conversion and squeezing using circuit QED, *Phys. Rev. Lett.* **95**, 140504 (2005).
 - [27] F. Marquardt, Efficient on-chip source of microwave photon pairs in superconducting circuit QED, *Phys. Rev. B* **76**, 205416 (2007).
 - [28] H. Wang, M. Hofheinz, M. Ansmann, R. C. Bialczak, E. Lucero, M. Neeley, A. D. O’Connell,

- D. Sank, J. Wenner, A. N. Cleland, and John M. Martinis, Measurement of the decay of fock states in a superconducting quantum circuit, *Phys. Rev. Lett.* **101**, 240401 (2008).
- [29] M. Hofheinz, E. M. Weig, M. Ansmann, R. C. Bialczak, E. Lucero, M. Neeley, A. D. O’Connell, H. Wang, J. M. Martinis and A. N. Cleland, Generation of fock states in a superconducting quantum circuit, *Nature* **454**, 310 (2008).
- [30] M. Mariantoni, F. Deppe, A. Marx, R. Gross, F. K. Wilhelm, and E. Solano, Two-resonator circuit quantum electrodynamics: A superconducting quantum switch, *Phys. Rev. B* **78**, 104508 (2008).
- [31] F. W. Strauch, K. Jacobs and R. W. Simmonds, Arbitrary control of entanglement between two superconducting resonators, *Phys. Rev. Lett.* **105**, 050501 (2010).
- [32] Q. P. Su, C. P. Yang and S. B. Zheng, Fast and simple scheme for generating NOON states of photons in circuit QED, *Scientific reports* **4**, (2014).
- [33] S. J. Xiong, Z. Sun, J. M. Liu, T. Liu, and C. P. Yang, Efficient scheme for generation of photonic NOON states in circuit QED, *Optics Letters* **40**, 2221 (2015).
- [34] M. Hua, M. J. Tao and F. G. Deng. Universal quantum gates on microwave photons assisted by circuit quantum electrodynamics, *Phys. Rev. A* **90**, 18824 (2014).
- [35] M. Hua, M. J. Tao and F. G. Deng, Quantum state transfer and controlled-phase gate on one-dimensional superconducting resonators assisted by a quantum bus, *Scientific reports* **6**, (2016).
- [36] A. N. Korotkov, Flying microwave qubits with nearly perfect transfer efficiency, *Phys. Rev. B* **84**, 014510 (2011).
- [37] E. A. Sete, E. Mlinar, and A. N. Korotkov, Robust quantum state transfer using tunable couplers, *Phys. Rev. B* **91**, 144509 (2015).
- [38] H. Wang, M. Mariantoni, R. C. Bialczak, M. Lenander, E. Lucero, M. Neeley, A. D. O’Connell, D. Sank, M. Weides, and J. Wenner *et al.*, Deterministic entanglement of photons in two superconducting microwave resonators, *Phys. Rev. Lett.* **106**, 060401 (2011).
- [39] S. J. Srinivasan, N. M. Sundaresan, D. Sadri, Y. Liu, J. M. Gambetta, T. Yu, S. M. Girvin, and A. A. Houck, Time-reversal symmetrization of spontaneous emission for quantum state transfer, *Phys. Rev. A* **89**, 033857 (2014).
- [40] J. Wenner et al., Catching Time-Reversed Microwave Coherent State Photons with 99.4% Absorption Efficiency, *Phys. Rev. Lett.* **112**, 210501 (2014).

- [41] C. P. Yang, Q. P. Su and S. Y. Han, Generation of Greenberger-Horne-Zeilinger entangled states of photons in multiple cavities via a superconducting qutrit or an atom through resonant interaction, *Phys. Rev. A* **86**, 022329 (2012).
- [42] C. P. Yang, Q. P. Su, S. B. Zheng, and S. Han, Generating entanglement between microwave photons and qubits in multiple cavities coupled by a superconducting qutrit, *Phys. Rev. A* **87**, 022320 (2013).
- [43] N. Ofek, A. Petrenko, R. Heeres, P. Reinhold, Z. Leghtas, B. Vlastakis, Y. Liu, L. Frunzio, S. M. Girvin, and L. Jiang *et al.*, Extending the lifetime of a quantum bit with error correction in superconducting circuits, *Nature* **536**, 441 (2016).
- [44] M. Mirrahimi, Z. Leghtas, V. V. Albert, S. Touzard, R. J. Schoelkopf, L. Jiang, and M. H. Devoret, Dynamically protected cat-qubits: a new paradigm for universal quantum computation, *New J. Phys.* **16**, 045014 (2014).
- [45] S. E. Nigg, Deterministic hadamard gate for microwave cat-state qubits in circuit QED. *Phys. Rev. A* **89**, 022340 (2014).
- [46] R. W. Heeres, P. Reinhold, N. Ofek, L. Frunzio, L. Jiang, M. H. Devoret, and R. J. Schoelkopf, Implementing a universal gate set on a logical qubit encoded in an oscillator, *arXiv:1608.02430*, (2016).
- [47] C. P. Yang, Q. P. Su, S. B. Zheng, F. Nori, and S. Han, Entangling two oscillators with arbitrary asymmetric initial states, *Phys. Rev. A* **95**, 052341 (2017).
- [48] C. Wang, Y. Y. Gao, P. Reinhold, R. W. Heeres, N. Ofek, K. Chou, C. Axline, M. Reagor, J. Blumoff, and K. M. Sliwa *et al.*, A Schrodinger Cat Living in Two Boxes, *Science* **352**, 1087 (2016).
- [49] J. Koch, T. M. Yu, J. Gambetta, A. A. Houck, D. I. Schuster, J. Majer, A. Blais, M. H. Devoret, S. M. Girvin, and R. J. Schoelkopf, Charge-insensitive qubit design derived from the Cooper pair box, *Phys. Rev. A* **76**, 042319 (2007).
- [50] D. Sank et al., Measurement-Induced State Transitions in a Superconducting Qubit: Beyond the Rotating Wave Approximation, *Phys. Rev. Lett.* **117**, 190503 (2016).
- [51] D. F. James and J. Jerke, Effective hamiltonian theory and its applications in quantum information, *Can. J. Phys.* **85**, 625 (2007).
- [52] M. Sandberg, C. M. Wilson, F. Persson, T. Bauch, G. Johansson, V. Shumeiko, T. Duty, and P. Delsing, Tuning the field in a microwave resonator faster than the photon lifetime, *Appl.*

- Phys. Lett. **92**, 203501 (2008).
- [53] Z. L. Wang, Y. P. Zhong, L. J. He, H. Wang, J. M. Martinis, A. N. Cleland, and Q. W. Xie, Quantum state characterization of a fast tunable superconducting resonator, Appl. Phys. Lett. **102**, 163503 (2013).
- [54] P. J. Leek, S. Filipp, P. Maurer, M. Baur, R. Bianchetti, J. M. Fink, M. Göppl, L. Steffen, and A. Wallraff, Using sideband transitions for two-qubit operations in superconducting circuits, Phys. Rev. B **79**, 180511 (2009).
- [55] M. Neeley, M. Ansmann, R. C. Bialczak, M. Hofheinz, N. Katz, Erik Lucero, A. O’Connell, H. Wang, A. N. Cleland and J. M. Martinis, Process tomography of quantum memory in a Josephson-phase qubit coupled to a two-level state, Nat. Phys. **4**, 523 (2008).
- [56] D. M. Lu and S. B. Zheng, Scheme for realizing Kerr nonlinearity in Cavity QED, Chin. Phys. Lett., **24**, 1567 (2007).
- [57] C. P. Yang, Q. P. Su, S. B. Zheng, and F. Nori, Crosstalk-insensitive method for simultaneously coupling multiple pairs of resonators, Phys. Rev. A **93**, 042307 (2016).
- [58] For a transmon qutrit, the $|g\rangle \leftrightarrow |f\rangle$ transition is much weaker than those of the $|g\rangle \leftrightarrow |e\rangle$ and $|e\rangle \leftrightarrow |f\rangle$ transitions. Thus, we have $\gamma_{fg}^{-1} \gg \gamma_{eg}^{-1}, \gamma_{fe}^{-1}$.